

COMPRESSION AND REDUCED REPRESENTATION TECHNIQUES FOR PATCH-BASED RELAXATION

GRAHAM HARPER* AND RAY TUMINARO†

Abstract.

Patch-based relaxation refers to a family of methods for solving linear systems which partitions the matrix into smaller pieces often corresponding to groups of adjacent degrees of freedom residing within patches of the computational domain. The two most common families of patch-based methods are block-Jacobi and Schwarz methods, where the former typically corresponds to non-overlapping domains and the latter implies some overlap. We focus on cases where each patch consists of the degrees of freedom within a finite element method mesh cell. Patch methods often capture complex local physics much more effectively than simpler point-smoothers such as Jacobi; however, forming, inverting, and applying each patch can be prohibitively expensive in terms of both storage and computation time. To this end, we propose several approaches for performing analysis on these patches and constructing a reduced representation. The compression techniques rely on either matrix norm comparisons or unsupervised learning via a clustering approach. We illustrate how it is frequently possible to retain/factor less than 5% of all patches and still develop a method that converges with the same number of iterations or slightly more than when all patches are stored/factored.

1. Introduction. Relaxation methods play a key role within multigrid linear solvers. Unfortunately, unsatisfactory convergence rates are often observed when simple relaxation schemes (e.g., point Jacobi) are employed within standard (e.g., geometric) multigrid algorithms on matrices associated with complex partial differential equations (PDEs). This limitation is perhaps most well-known for saddle-point matrices, which arise from constrained PDEs systems such as the incompressible Navier-Stokes equations (INS) [7]. However, difficulties also emerge in other scenarios, even for symmetric positive definite matrices such as those coming from edge element discretizations of $\nabla \times \nabla u + \alpha u$ where α is a small positive constant. For this reason, many researchers have considered sophisticated relaxation methods based on the notion of patches, c.f. [8, 23, 2, 15, 10, 18, 6, 1]. Additionally, software specifically devoted to providing patch relaxation methods can be found in [11]. Patch methods can be viewed as a form of overlapping Schwarz domain decomposition, though in the multigrid context the patches or subdomains are small relative to subdomains commonly used in domain decomposition. Specifically, patch relaxation centers on solving many small linear systems that each correspond to a subset of equations of the large matrix. Perhaps one of the most well-known patch relaxation schemes is the Vanka method for incompressible flow [23], which has also been extended to magnetohydrodynamics (MHD) systems [6, 1]. While multigrid with patch relaxation often yields satisfactory convergence rates for many applications including many INS and MHD simulations, it comes at a significant cost in both storage and computation.

The main contribution of this article is the development of a family of new approximate patch-based relaxation methods that detect and exploit structure within a linear system. In particular, we analyze the spectral properties of patches in order to group or cluster similar patches together, and thus reduce the total number of patches required to solve the system. While clustering methods have been developed for matrix-variate data using density-based approaches [14, 12], our clustering strategy instead focuses on the spectral approximation qualities of the solver. This enables us to only factor/store a subset of patches in the setup phase and reuse data

*Sandia National Laboratories, (gbharpe@sandia.gov)

†Sandia National Laboratories, (rstumin@sandia.gov)

(stored factorizations) in the solve phase. In some sense, this is a dimension reduction technique for linear systems, similar in motivation to tensor decompositions [17] or low-rank approximations [13] as it greatly reduces the necessary data storage while increasing computational speed in our case. However, it is an approximate method, as we allow the reconstruction to be inexact at the cost of relaxation method accuracy. Approximate patch-based relaxation is based on the idea that a stored factorization can be used to approximate the true factorizations of similar patches. Of course, it is essential that overall convergence rates do not suffer significantly. These convergence rates ultimately depend on the set of patches used to create the subset of stored factorizations and how all patch solves are approximated using the stored factorizations. A criterion is proposed for measuring how well a computed factorization approximates the factorization of another patch matrix. This criterion is then used to identify patch subsets or to cluster patches together. Here, the idea is to employ a single factorization for all patches within the same cluster during the algorithm’s solve phase. This paper’s intent is to show the potential behind this new family of patch relaxation methods and to illustrate some initial approaches to determine and employ patch subsets. Future work will consider more sophisticated compression algorithms to further reduce storage costs as well as alternative algorithms that are more efficient during the setup phase.

In this paper, we focus on applications where the underlying discretization is high order. In this scenario, patch relaxation can be useful in conjunction with algebraic multigrid (AMG) due to the fact that direct application of AMG to high-order discretizations is often problematic. Instead, a common alternative is to develop a composite preconditioner that applies AMG only to a low-order discretization in conjunction with the application of patch relaxation to the high-order discretization. This approach is particularly useful with advanced discretizations (e.g., discontinuous Galerkin methods) where AMG might only be applied to a first-order continuous Galerkin finite element method, c.f. [4, 22, 5]. Other related applications include matrix-free approaches, which do not store the entire sparse discretization matrix and are essential in some applications due to storage limitations. Matrix-free approaches are particularly attractive for high-order discretizations as the number of matrix nonzeros may be so large that the discretization order would need to be reduced/limited in order to actually store the entire high-order discretization matrix. Unfortunately, the amount of memory required to store all the overlapping patch factors is often comparable to the memory needed to store the high-order discretization matrix. Thus, storing the patch factors defeats the low-storage advantage of a matrix-free approach. Further, an on-the-fly approach to patch relaxation is very costly. On-the-fly patch relaxation requires that a factorization be computed each time it is needed to solve a patch sub-problem. This means that during the solve phase an $O(p_s^3)$ Gaussian elimination algorithm must be repeatedly employed as opposed to an $O(p_s^2)$ backsolve algorithm that is used when a factorization is already computed. Here, p_s is the patch size or number of unknowns within a patch. If each patch corresponds to all unknowns within a single computational cell, $p_s = q(p + 1)^d$ when p^{th} -order Lagrange polynomial functions are used to discretize systems with q PDEs on d -dimensional tensor (quadrilateral/hexahedral) meshes. It follows that p_s can easily exceed 500 in many scenarios.

While this paper focuses on exploiting structure and reducing patch storage for high-order applications, we note that there may also be further significant gains associated with reusing patch factorizations when bandwidth/cache performance issues are considered on advanced computing hardware, especially on GPUs. While it is

often not possible to simultaneously keep all patch factorizations in some type of fast-access memory with traditional patch methods, it should be possible to keep a subset of patch factorizations in fast-access memory during the backsolves associated with multiple right hand sides. Finally, we remark that while we consider patch relaxation within multigrid for high-order discretizations, patch schemes are also useful as preconditioners (without multigrid), especially for time dependent multiphysics problems.

This paper proceeds by formally defining a traditional patch relaxation method in Section 2. Section 3 describes the approximate patch relaxation idea and provides an associated minimization function that guides the compressed representation used to approximate patch inverses. In Section 3.1 a simple algorithm is presented to identify a subset of patch matrices whose factorizations can be used to approximate other patch matrix inverses. A more sophisticated algorithm is given in Section 3.2 that leverages clustering ideas from machine learning. Numerical results are presented in Section 4 illustrating the efficacy of the compressed representation when preconditioning high-order discretization problems. Finally, Section 5 provides a conclusion and discusses additional work needed to mature the basic idea.

2. Patch-based smoothers background. A classical Jacobi iterative method can be viewed as a non-overlapping patch algorithm where each degree of freedom is treated as its own patch matrix. A single Jacobi iteration applied to the $n \times n$ linear system

$$Ax = b$$

corresponds to updating each solution unknown independently via

$$x_i^{(m+1)} = x_i^{(m)} + A_{ii}^{-1} \left(b_i - \sum_{j=1}^n A_{ij} x_j^{(m)} \right), \quad i = 1, \dots, n$$

where $x^{(m)}$ denotes the current approximate solution after m Jacobi iterations. When applied with damping coefficient ω , Jacobi can be written succinctly as

$$\mathbf{x}^{(m+1)} = \mathbf{x}^{(m)} + \omega D^{-1} (\mathbf{b} - A\mathbf{x}^{(m)})$$

where D is a diagonal matrix whose only nonzeros correspond to $D_{ii} = A_{ii}$. While the Jacobi iteration is inexpensive to store and fast to apply, it does not scale well for problems involving complex multiphysics interactions or some high-order polynomial discretizations. A more sophisticated block Jacobi iterative scheme is obtained by changing the definition of D to instead be a block diagonal matrix whose nonzero entries are defined by $D_{ij} = A_{ij}$. Typically, the rows/columns of a block might include all degrees of freedom (DoFs) that are defined at the same spatial location for a PDE system or might include all DoFs defined at spatial locations within a small local neighborhood. A more general and robust patch relaxation procedure can be defined when the small neighborhoods are allowed to overlap as depicted on the left side of Figure 1, though this can no longer be represented by a block diagonal matrix D due to the overlap. This class of algorithms is also referred to as overlapping Schwarz methods. The right side of Figure 1 illustrates a single Vanka patch to solve the two dimensional incompressible Stokes equations. Here, each patch coincides with one pressure DoF and includes all velocity DoFs in the four elements that contain the pressure DoF.

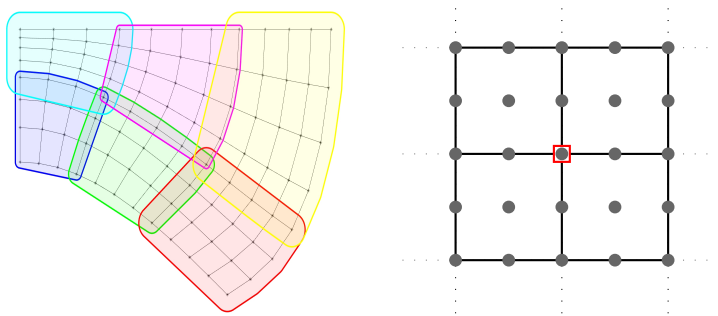


FIG. 1. *Left: sample mesh with 6 patches. Right: 1 Stokes flow Vanka patch for a $\mathbb{Q}_2/\mathbb{Q}_1$ discretization that includes a pressure DoF \square and all velocity DoFs \bullet residing within elements containing the pressure DoF.*

To formally define patch relaxation, we introduce the $p_s \times n$ boolean restriction matrix V_k , $k = 1, \dots, n_p$. Here, we assume that all n_p patches are of the same size p_s (often the case when preconditioning high-order discretization matrices). Each nonzero V_k entry is given by $(V_k)_{ij} = 1$ if and only if global degree of freedom j corresponds to local patch degree of freedom i . Restricting the matrix A to the k^{th} patch is defined by

$$A_k = V_k A V_k^T, \quad k = 1, \dots, n_p.$$

An $n \times n$ diagonal weight matrix $W = \left(\sum_{\ell=1}^{n_p} V_\ell^T V_\ell \right)^{-1}$ is defined to average solutions from overlap regions. This is equivalent to taking W_{ii} as the reciprocal of the number of patches that include the i^{th} global DoF. A patch preconditioner M^{-1} is then given by

$$(2.1) \quad M^{-1} = W \sum_{k=1}^{n_p} V_k^T A_k^{-1} V_k.$$

Therefore, applying $M^{-1}r$ corresponds to the restriction of r to each patch, performing a patch solve, injecting the solution back to the larger problem, and then combining/averaging the results.

Remark: While we define patch relaxation in terms of a single patch size p_s , this extends to patches of different sizes. The algorithms developed later in Section 3 may be applied to each group of same-size patches independently.

Many different patch choices are possible. As already noted, Vanka patches have proved useful for the incompressible Navier Stokes equations. Arnold-Faulk-Winther patches [2] are useful for some electromagnetics applications to precondition operators where the underlying PDE has the form $\nabla \times \nabla u + \alpha u$. Other types of patches can be useful for some MHD formulations. In this paper, our definition of a patch is the smallest computational domain with exploitable regular structure. For many discretizations and applications, this domain is exactly a mesh cell, which we recall may contain as many as $p_s = q(p+1)^d$ degrees of freedom when solving q PDEs with p^{th} -order Lagrange polynomials on a d -dimensional cube.

Figure 2 highlights the different types of patches, such as the vertex-star and cell-centered patches, which are discussed in [8], versus our cell-restricted patch. Vertex-star patches are generally the most robust for patch-based relaxation methods as the

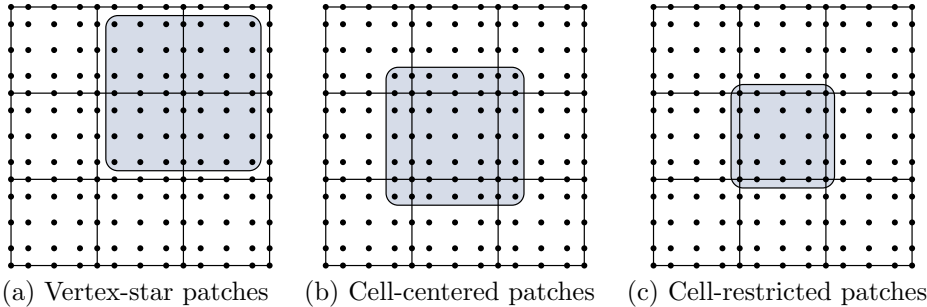


FIG. 2. Comparison of different patch methods on a quadrilateral grid with a $p = 4$ discretization.

polynomial degree p increases; however, a vertex-star patch may have varying sizes depending on the connectivity of the vertex within the mesh. This means there is irregularity in patch size on unstructured grids. The cell-centered patch includes a halo from its neighbors, which is generally more robust than cell-restricted patches. We remark that stencil irregularity may be handled by grouping alike-sized patches together before applying the algorithms in the following section, but both vertex-star and cell-centered patches tend to also require invasive information from the application beyond the supplied linear system. From here forward, we utilize the cell-restricted patches shown in (c) of Figure 2, as we can easily detect them by searching a linear system for rows with $q(p + 1)^d$ symbolically nonzero entries for tensor-product cell shapes without requiring additional information from the application that generated the system. This may be adjusted accordingly depending on the cell shape and discretization.

We focus on preconditioning high-order discretizations via a combination of patch preconditioning and multigrid applied to a first-order discretization developed on the same mesh used for the high-order discretization. Specifically, an additive combination preconditioner has the form

$$(2.2) \quad M_{\text{combo}}^{-1} = M^{-1} + P_0 M_{\text{amg}}^{-1} R_0$$

where M^{-1} is the patch method, P_0 interpolates solutions from the low order representation to the high-order representation, M_{amg}^{-1} denotes the first order AMG preconditioner and R_0 restricts residual from the high-order representation to the low order representation. Section 4 further discusses M_{combo}^{-1} . We close this section by noting that there are other AMG approaches to high-order discretizations that avoid the need for a patch preconditioner. One noteworthy possibility is to define a first order discretization using a refined mesh such that the spatial locations associated with unknowns on both the first order and high-order systems coincide [16, 19, 20]. Another possibility instead uses p -multigrid by creating a hierarchy of intermediate discretizations and reducing the order of approximation by only one as we proceed through the hierarchy [21].

3. Approximate Patch Smoothers. To develop an approximate patch preconditioner, we need to define a subset of factored or inverse patch matrices

$$\mathcal{B} = \{B_1^{-1}, B_2^{-1}, \dots, B_{m_p}^{-1}\}$$

and to identify a means of approximating each of the true patch inverses using only \mathcal{B} . Here, $m_p (\leq n_p)$ denotes the total number of computed inverses. While it is possible to

consider sophisticated schemes that combine several B_j^{-1} to approximate the j^{th} patch inverse, we restrict ourselves to the simplest case where only a single factorization is used, i.e. $A_j^{-1} \approx B_{\phi(j)}^{-1}$. In this case, a mapping $\phi : \{1, \dots, n_p\} \rightarrow \{1, \dots, m_p\}$ must be determined. We will refer to \mathcal{B} as the inverse database, but it may also be thought of as a compressed representation or sparse approximation of the true patch inverses A_i^{-1} , $i = 1, \dots, n_p$. Ultimately, \mathcal{B} and $\phi(\cdot)$ define an approximate preconditioner

$$(3.1) \quad \tilde{M}^{-1} = W \sum_{k=1}^{n_p} V_k^T B_{\phi(k)}^{-1} V_k.$$

When \tilde{M} is employed as a stand-alone preconditioner, we seek a well conditioned $\tilde{M}^{-1}A$ using a \mathcal{B} such that m_p is not too large. When \tilde{M} is used within multigrid, we instead seek a relaxation error smoother operator $I - \omega \tilde{M}^{-1}A$ (with damping parameter ω) that damps errors which cannot be well-represented on the first-order mesh. The difference between the ideal operator $I - \omega M^{-1}A$ and the approximate operator $I - \omega \tilde{M}^{-1}A$ on patch i is given by

$$V_i \left((I - \omega M^{-1}A) - (I - \omega \tilde{M}^{-1}A) \right) V_i^T = \omega V_i W \sum_{k=1}^{n_p} \left(V_k^T (A_k^{-1} - B_{\phi(k)}^{-1}) V_k \right) A V_i^T.$$

This results in an error term of the form $(A_i^{-1} - B_{\phi(i)}^{-1}) A_i = I - B_{\phi(i)}^{-1} A_i$ after we have ignored leading constants and discarded terms that appear due to overlap. Therefore, a good approximation would aim to reduce $\sum_{k=1}^{n_p} \|I - A_k B_{\phi(k)}^{-1}\|_2^2$, noting symmetric matrices may be commuted in the norm. We consider the following minimization problem: seek a database \mathcal{B} and mapping $\phi(\cdot)$ minimizing $\mathcal{L}(\mathcal{B}, \phi)$, where

$$(3.2) \quad \mathcal{L}(\mathcal{B}, \phi) = \beta |\mathcal{B}| + \sum_{k=1}^{n_p} \|I - A_k B_{\phi(k)}^{-1}\|_2^2$$

where the A_k and $\beta > 0$ are given, $|\cdot|$ is set cardinality, and $\|\cdot\|_2$ is the matrix 2-norm. Clearly, the second term is minimized when each B_k^{-1} exactly approximates all patch inverses assigned to it (i.e., for all j, k such that $\phi(k) = j$, $B_j^{-1} = A_k^{-1}$). However, the first term penalizes the objective based on the size of \mathcal{B} . Thus, the two terms in (3.2) balance the storage costs (and computation costs) associated with having a large set of approximate inverses against the quality of the inverse approximations.

Remark: The entrywise difference Frobenius norm $\|A_k - B_{\phi(k)}\|_F^2$ or the entrywise absolute difference ℓ_1 norm are among the cheapest to compute since these may be done before computing each $B_{\phi(k)}^{-1}$, but using such entrywise differences also provides less information about the quality of approximation than, for example, comparing the spectrum of $A_k B_{\phi(k)}^{-1}$ to the identity. For these reasons, despite the nonsymmetry, we use the 2-norm as it may be computed exactly by a small SVD or approximated by a few steps of the power method applied to $I - A_k B_{\phi(k)}^{-1}$.

Remark: The minimization problem (3.2) guarantees a minimum exists, and the ϕ mapping must be onto to be a minimizer, but does not allow for a unique minimizer. The minimum is guaranteed to exist as the objective function is bounded below by β in the case of \mathcal{B} with only one entry. Furthermore, in the case of a minimizer, all entries of the database \mathcal{B} must be matched with at least one A_i patch, implying the map ϕ must be onto. If that were not the case, the objective function value could simply

be decreased by removing unnecessary patches. This means it is logical to consider constructive approaches for computing \mathcal{B} in practice. However, the minimizer is not unique because any permutation of a database that minimizes this objective function is also a minimizer. This could be rectified by imposing additional conditions on the ordering of terms in \mathcal{B} . These technical details are not critical here so long as the underlying minimization algorithm is not affected by permutations in the database.

Notice that solving the above minimization problem could be computationally expensive, especially given the fact that $\mathcal{L}(\mathcal{B}, \phi)$ is not differentiable as $|\mathcal{B}|$ takes on only integer values. However, an exact minimizer is not necessary, only a solution that gives acceptable convergence rates for a reasonable cost. Furthermore, there are a number of ways in which an inexpensive initial guess can be used to start a minimization process.

3.1. Patch Equality Compression. When relatively small values of β are considered, the $\mathcal{L}(\mathcal{B}, \phi)$ minimization problem essentially attempts to exactly satisfy the first term in (3.2). While this might lead to a large $|\mathcal{B}|$ for general unstructured/-variable coefficient PDE problems, this is not the case for homogeneous coefficient PDEs on regular meshes, as the majority of the patch matrices (excluding boundary conditions) are identical. This type of small β or patch equality compression scenario is also beneficial for problems with piecewise-constant variations in materials. These problems come up frequently when modeling geologic or crystalline structure of materials or in semiconductor simulations. One simple approach that avoids the explicit $\mathcal{L}(\mathcal{B}, \phi)$ minimization problem is given in Algorithm 3.1. This algorithm requires $O(n_p m_p)$ operations as each patch must be checked against the current \mathcal{B} to see if there is already a suitable match or whether \mathcal{B} should be enlarged.

Algorithm 3.1 Patch Tolerance Construction of \mathcal{B} and $\phi()$

```

1: Input: patches  $\{A_1, A_2, \dots, A_{n_p}\}$ , tolerance  $\varepsilon$ 
2:  $\mathcal{B} := \{\}$ ,  $\vec{\phi} = \vec{0}$ 
3: for  $i = 1, 2, \dots, n_p$  do
4:   match:=false;
5:   for  $j = 1, 2, \dots, |\mathcal{B}|$  do
6:     if  $\|I - A_i B_j^{-1}\|_2 < \varepsilon$  then           // If a suitable match is found...
7:       match=true,  $\phi(i) = j$ , break;           // save the index, skip to next patch
8:     end if
9:   end for
10:  if match==false then                           // If no suitable match is found...
11:    append  $A_i^{-1}$  to  $\mathcal{B}$ ,  $\phi(i) = |\mathcal{B}|$ ;           // append database,  $m_p$  incremented
12:  end if
13: end for
14: Output:  $\mathcal{B} = \{B_1^{-1}, B_2^{-1}, \dots, B_{m_p}^{-1}\}$ ,  $\vec{\phi}$ 

```

When $m_p \ll n_p$, the complexity of Algorithm 3.1 might be satisfactory. Alternatively, complexity could be reduced to $O(n_p \log(m_p))$ by storing the B_k^{-1} matrices in some sorted fashion (e.g., based on $\|B_k\|_2$). A faster logarithmic search is then accomplished by first identifying a subset of \mathcal{B} matrices to search and then changing the for loop on Line 5 so that only matrices in this subset are tested. Additionally, while this algorithm as written exits upon the first found match, such behavior makes it sensitive to permutations of the input data in cases with large ε . Instead, one may

match A_i with the closest of many B_j satisfying Line 6. These modifications and other forms of acceleration for this approach will be considered in future work.

3.2. Patch Clustering. As noted, Algorithm 3.1 can be adapted so that it is relatively inexpensive. However, Algorithm 3.1 prioritizes the minimization of accuracy term in Equation 3.2. When the number of database entries is a constraint, and the first term of $\mathcal{L}(\mathcal{B}, \phi)$ is main priority for minimization, instead one may consider clustering algorithms where the number of clusters is specified a priori. In this paper, we consider perhaps one of the simplest based on k -means clustering. k -means starts with an initial set of cluster assignments and computes an associated mean for each cluster. The algorithm alternates between updating the cluster assignments by identifying the points closest to the mean and then by updating the means given the new cluster assignments. In our context, we define the distance metric on patch matrices by

$$(3.3) \quad d(A, B) = \|I - AB^{-1}\|_2.$$

Cluster means are then computed by the entry-wise mean

$$(3.4) \quad B_i = |\phi^{-1}(i)|^{-1} \sum_{k \in \phi^{-1}(i)} A_k,$$

where $\phi^{-1}(i)$ is the pre-image of i under ϕ and $|\cdot|$ is set cardinality. Because the map ϕ must be onto, this pre-image is always well-defined. Algorithm 3.2 summarizes the k -means algorithm.

Algorithm 3.2 Spectral Clustering Construction of \mathcal{B} and $\phi()$

```

1: Input: patches  $\{A_1, A_2, \dots, A_{n_p}\}$ , database size  $m_p$ 
2:  $\vec{\phi} = \text{randperm}(n_p, m_p)$ ; // Initialize clusters via random permutation
3: for  $j = 1, \dots, m_p$  do
4:    $B_j^{-1} = A_{\phi(j)}^{-1}$ ; // Assign cluster representatives
5: end for
6: converged=false;
7: while converged==false do
8:   converged=true;
9:   for  $i = 1, \dots, n_p$  do // For each patch...
10:    for  $j = 1, \dots, m_p$  do // For each cluster...
11:       $d_j = d(A_i, B_j)$ ; // compute distance to cluster center
12:    end for
13:    if  $\phi(i) \neq \text{argmin}_j(d_j)$  then; // If nearest cluster changed...
14:      converged=false; // clustering is not converged,
15:       $\phi(i) = \text{argmin}_j(d_j)$ ; // update closest cluster assignment
16:    end if
17:  end for
18:  if converged==false then // If not converged...
19:    for  $j = 1, \dots, m_p$  do
20:      recompute  $B_j^{-1}$ ; // update cluster representatives
21:    end for
22:  end if
23: end while
24: Output:  $\mathcal{B} = \{B_1^{-1}, B_2^{-1}, \dots, B_{m_p}^{-1}\}$ ,  $\vec{\phi}$ 

```

We note that Algorithm 3.2 provides one simple method for determining when to end the algorithm, but there are other possible choices, such as maximum iteration limits, which are trivial to implement. Line 11 defines the distance between patches, and line 20 refers to recomputing B_i^{-1} , which can be done several different ways. We will break this algorithm into three sub-algorithms depending on how this is addressed:

- **Entrywise k -means** computes $d(A_i, B_j) = \|A_i - B_j\|_{\ell_1}$ and defines B_j^{-1} as the inverse of the entrywise average over a cluster.
- **Spectral k -means** computes $d(A_i, B_j) = \|I - A_i B_j^{-1}\|_2$ and defines B_j^{-1} as the inverse of the entrywise average over a cluster.
- **Variance-minimizing clustering** computes $d(A_i, B_j) = \|I - A_i B_j^{-1}\|_2$ and defines B_j^{-1} as the inverse of the cluster member which minimizes the in-cluster variance.
- **Bootstrapping** initializes clustering by first computing Algorithm 3.1 and then uses the resulting \mathcal{B} as initial clusters for Algorithm 3.2. We expect this to perform slightly better than Algorithm 3.1 on its own.

As the algorithm is written, there are potential difficulties with computing cluster assignments in this fashion, and future work will consider alternatives. One obvious problem concerns the preservation of boundary conditions that sometimes appear in local patches. Boundary conditions appear in these patches as a row with only one nonzero entry, and therefore any entrywise averaging scheme between a matrix with a boundary condition and a matrix without a boundary condition will immediately result in a matrix without a boundary condition, destroying the original boundary condition information. In practice, we adapt our method by partitioning the patch matrices dataset based on the presence of a boundary condition, which splits the dataset into an “interior” and a “boundary.” Again, due to similar issues with entrywise averaging, we partition the boundary further so that each boundary partition only contains matrices which have boundary conditions in the same rows. In theory, there are possibly 2^{p_s} different partitions of the dataset; however, in practice there are 9 on a two-dimensional square domain (associated with four corners, four edges, and one interior of the domain) and 27 on a three-dimensional cube domain (associated with eight corners, twelve edges, six faces, and one interior of the domain). We then independently cluster on each partition, and the final cluster assignments are simply the union of all partitioned clustering results. In Section 4, we divide the number of clusters between boundary types so that the number of patches is roughly proportional to the number of patches in the group. One possible nearly equivalent alternative to the partitioning approach would be to redefine the distance metric with an additional term that heavily penalizes cases where the number of nonzeros in a row of A and a row of B are different. This could be used in conjunction with some initialization of $\phi()$ to ensure that no initial clusters violate this nonzero condition.

There are several possible improvements that one can consider to the basic k -means algorithms to reduce the overall cost, automatically determine a cluster size, and to improve to the quality of the clusters found via the algorithm. The Bootstrapping method effectively determines the number of clusters for k -means and greatly reduces the number of k -means iterations needed. It also eliminates the need to partition patches based on their interior or boundary orientation. Furthermore, cost may be greatly improved by performing minibatch k -means, although the algorithm is typically less stable and depends on an adequate representation of the group by the random sample [3]. In addition, there are a number of advanced possibilities that are somewhat more closely tied to our application.

For linear problem sequences (e.g., from time marching or nonlinear solvers), there are techniques to update or revise an existing set of clusters to account for the new data. For example, one may initialize a database using the results from the previous time step to greatly accelerate the convergence of the clustering algorithm. However, this also depends on other factors such as the nonlinearity of the system.

Additionally, there are interesting combinations of clustering algorithms with deep learning neural networks that may be useful to compress the representation before the clustering algorithms, determine the number of clusters, and allow for more general type of cluster regions to be determined [9]. We have initiated some work in the deep learning area, but this is beyond the scope of the current manuscript.

4. Numerical Results. We now consider several different scenarios to demonstrate our ability to identify and exploit structure in various scenarios. For multigrid applications, a two dimensional Poisson problem is considered with varying coefficients

$$-\nabla \cdot (\rho(x, y) \nabla u) = f$$

on a unit square $[0, 1]^2$ with Dirichlet boundary conditions. Finite elements are employed on a regular quadrilateral mesh using Lagrange polynomial basis functions with polynomial degree $p \leq 5$. Example 1 corresponds to a smoothly varying situation where $\rho()$ is given by a product of sine functions with a constant offset from zero and is depicted on the left side of Figure 3. Example 2, shown on the right side of Figure 3, corresponds to a multiple material case where $\rho()$ is a piecewise constant function. Example 3 corresponds to the case $\rho(x, y) = 1$ and is used primarily for the performance discussion, and Example 4 presents discussion on how one may consider the viability of extending such an algorithm to more complex problems such as Burgers' equation with a shock formation.

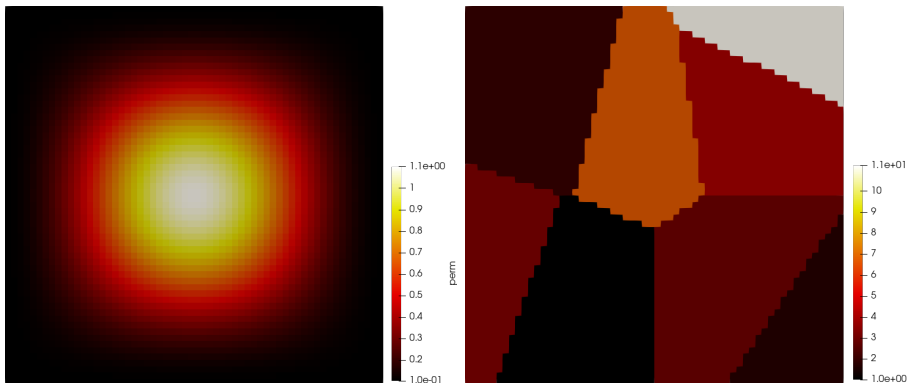


FIG. 3. Graphical illustration of $\rho(x, y)$ for a smooth case (left) and for a discontinuous case (right)

Experiment 1 patch compression for the smooth case.

Experiments 1 and 2 are performed in Matlab using GMRES (with a restart size of 20) in conjunction with M_{combo}^{-1} . Again, each patch corresponds to one finite element, so there are 3600 true patches on a 60×60 mesh. A direct solver applied to the matrix $R_0 A P_0$ is used for M_{amg}^{-1} , though we have also performed experiments with AMG that give similar convergence profiles. Here, A is the high-order discretization matrix. The interpolation operator P_0 corresponds to linear interpolation viewing

| | | | | | | | | | |
|---------|---------------------------|------|----|----|----|----|----|----|----|
| $p = 2$ | Algorithm\Database Size | 3600 | 74 | 35 | 18 | 15 | 13 | 7 | 6 |
| | Greedy Tolerance 3.1 | 11 | 12 | 13 | 14 | 17 | 26 | 61 | 68 |
| | Spectral k -means 3.2 | 11 | 12 | 12 | 14 | 16 | 17 | – | – |
| | Var-Minimizing Clustering | 11 | 12 | 12 | 13 | 14 | 15 | – | – |
| | Entrywise k -means | 11 | 11 | 12 | 12 | 14 | 16 | – | – |
| $p = 3$ | Algorithm\Database Size | 3600 | 71 | 34 | 18 | 15 | 13 | 8 | 6 |
| | Greedy Tolerance 3.1 | 12 | 13 | 13 | 15 | 18 | 26 | 58 | 69 |
| | Spectral k -means 3.2 | 12 | 12 | 12 | 15 | 17 | 18 | – | – |
| | Var-Minimizing Clustering | 12 | 12 | 12 | 13 | 14 | 15 | – | – |
| | Entrywise k -means | 12 | 12 | 12 | 12 | 14 | 16 | – | – |
| $p = 4$ | Algorithm\Database Size | 3600 | 71 | 34 | 18 | 15 | 13 | 8 | 7 |
| | Greedy Tolerance 3.1 | 14 | 14 | 15 | 17 | 20 | 29 | 68 | 67 |
| | Spectral k -means 3.2 | 14 | 14 | 14 | 17 | 19 | 20 | – | – |
| | Var-Minimizing Clustering | 14 | 14 | 14 | 15 | 16 | 17 | – | – |
| | Entrywise k -means | 14 | 14 | 14 | 14 | 16 | 18 | – | – |
| $p = 5$ | Algorithm\Database Size | 3600 | 73 | 35 | 18 | 15 | 13 | 9 | 7 |
| | Greedy Tolerance 3.1 | 15 | 16 | 17 | 19 | 22 | 32 | 78 | 76 |
| | Spectral k -means 3.2 | 15 | 16 | 16 | 19 | 21 | 22 | – | – |
| | Var-Minimizing Clustering | 15 | 15 | 16 | 17 | 18 | 19 | – | – |
| | Entrywise k -means | 15 | 15 | 15 | 16 | 18 | 20 | – | – |

TABLE 1

Comparison of multigrid iteration counts for varying database algorithms, database sizes, and polynomial degrees applied to Example 1 on a 60×60 mesh.

the spatial location of the DoFs in a high-order discretization as defining a fine mesh. Finally, $R_0 = P_0^T$. The function $\rho(x, y)$ is defined by $\rho(x, y) = \sin^2(\pi x) \sin^2(\pi y) + 0.1$. The right hand side is chosen so that the solution is given by $u = \sin(\pi x) \sin(\pi y)$. The GMRES iterative process is started with a zero initial guess and convergence is declared when the initial residual is reduced by 10^{-8} . Table 1 gives results for a variety of algorithms from Section 3 applied to Example 1 on a 60×60 mesh. and clustering is not run when the database size is less than 10 as the total number of clusters is split across the 8 boundary conditions and 1 interior, as indicated by – entries.

By examining Table 1 one can see that with only 34 or 35 patches the total number of GMRES iterations increases by no more than 2 iterations over the case when all 3600 patches are used, regardless of the choice of p . That is, acceptable convergence rates are attained even while retaining less than one percent of all patches. However, as the database size is reduced to 10 patches or less, convergence begins to degrade significantly for Algorithm 3.1.

Experiment 2 patch compression for the discontinuous case.

The right hand side is chosen so that the solution is again given by $u = \sin(\pi x) \sin(\pi y)$, ρ is discontinuous piecewise constants, and the iterative GMRES process is started with a zero initial guess and a tolerance of 10^{-8} . Table 2 gives multigrid iteration counts for a variety of algorithms from Section 3, database sizes, and polynomial degrees applied to Experiment 2 on a 60×60 mesh, and again clustering is not run when the database size is less than 10.

Interestingly, we see that Algorithm 3.1 outperforms any variation of clustering specified in Section 3 except for the bootstrapped clustering, which we ran only in

| | | | | | | | | | |
|---------|-----------------------------|------|-----|-----|-----|----|----|----|----|
| $p = 2$ | Algorithm\Database Size | 3600 | 131 | 113 | 96 | 52 | 25 | 5 | 3 |
| | Greedy Tolerance 3.1 | 11 | 12 | 12 | 14 | 17 | 22 | 47 | 52 |
| | Spectral k -means 3.2 | 11 | 17 | 19 | 19 | 26 | 27 | – | – |
| | Var-Minimizing Clustering | 11 | 20 | 20 | 20 | 29 | 31 | – | – |
| | Entrywise k -means | 11 | 12 | 17 | 17 | 26 | 31 | – | – |
| $p = 3$ | Algorithm\Database Size | 3600 | 131 | 114 | 100 | 59 | 32 | 8 | 5 |
| | Greedy Tolerance 3.1 | 12 | 12 | 13 | 14 | 17 | 26 | 48 | 50 |
| | Spectral k -means 3.2 | 12 | 20 | 26 | 26 | 34 | 35 | – | – |
| | Var-Minimizing Clustering | 12 | 24 | 24 | 24 | 32 | 32 | – | – |
| | Entrywise k -means | 12 | 13 | 19 | 19 | 29 | 33 | – | – |
| $p = 4$ | Algorithm\Database Size | 3600 | 130 | 114 | 103 | 70 | 36 | 12 | 9 |
| | Greedy Tolerance 3.1 | 14 | 14 | 15 | 15 | 19 | 28 | 51 | 53 |
| | Spectral k -means 3.2 | 14 | 23 | 32 | 32 | 33 | 38 | 36 | – |
| | Var-Minimizing Clustering | 14 | 27 | 27 | 27 | 27 | 38 | 37 | – |
| | Entrywise k -means | 14 | 16 | 22 | 22 | 22 | 35 | 37 | – |
| $p = 5$ | Algorithm\Database Size | 3600 | 130 | 116 | 103 | 78 | 38 | 15 | 10 |
| | Greedy Tolerance 3.1 | 15 | 16 | 16 | 17 | 21 | 29 | 60 | 64 |
| | Spectral k -means 3.2 | 15 | 25 | 35 | 30 | 35 | 40 | 43 | 39 |
| | Var-Minimizing Clustering | 15 | 28 | 28 | 54 | 47 | 40 | 40 | 44 |
| | Bootstrapped Var-Minimizing | 15 | 16 | 16 | 17 | 22 | 26 | 44 | 39 |
| | Entrywise k -means | 15 | 18 | 25 | 25 | 25 | 38 | 40 | 38 |

TABLE 2

Comparison of multigrid iteration counts for varying database algorithms, database sizes, and polynomial degrees applied to Experiment 2 on a 60×60 mesh.

the case of $p = 5$. Bootstrapping performed best for $|\mathcal{B}| = 38, 15, 10$. It required the same number of iterations as Algorithm 3.1 for other $|\mathcal{B}|$ sizes, except $|\mathcal{B}| = 78$ where it required one additional iteration. With $|\mathcal{B}| = 130$ or 131 , Algorithm 3.1 costs at most one additional solver iteration than using all 3600 patches, while the clustering algorithms cost significantly more iterations and do not scale as well. We suspect this is due to the piecewise constant nature of the problem, which makes clustering less effective.

Figure 4 depicts the clusters identified by the two respective algorithms. Here, one can see that the found clusters generally match the $\rho()$ functions depicted in Figure 3.

Experiment 3 Timings for $\rho(x, y) = 1$ problem.

While our focus is on reduction in the size of the dataset with little loss of accuracy, we did investigate timings using a variant of the greedy database compression scheme described by Algorithm 3.1 in the `DatabaseSchwarz` class of the `Ipack2` preconditioning package, and we called it from the `MueLu` multigrid package. Both packages are part of the C++ Trilinos framework. We utilized this preconditioner as a simple smoothing iteration of the form

$$x \leftarrow x + \omega M^{-1}r,$$

where $r = b - Ax$ is the residual.

For this, we use a variation of Algorithm 3.1 which checks $\|A_i - B_j\|_{\ell_1} < \varepsilon$ for simplicity. In this case, we consider a $20 \times 20 \times 20$ finite element discretization with $p = 5$ polynomial degree, yielding 8000 patches where each patch is of size 216×216 .

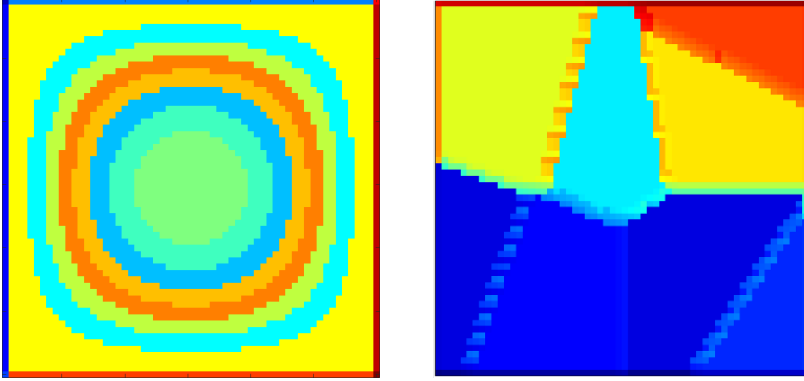


FIG. 4. Visualization of ϕ mapping for $p = 5$ determined by Algorithm 3.2 spectral k-means for Experiment 1 (left with 16 clusters) and by Algorithm 3.1 for Experiment 2 (right with 130 unique entries)

| Configuration | Setup time (s) | Apply time (s) |
|----------------|----------------|----------------|
| No compression | 287.4 | 64.5 |
| Compression | 262.0 | 49.4 |

TABLE 3

Experiment 3: comparison of timings in the case of no compression and compression

We utilize this approach as a preconditioner inside a GMRES solver with a database tolerance of $\varepsilon = 10^{-7}$ and a GMRES tolerance of 10^{-7} as well. We compare timings in two different scenarios, each taking 39 iterations to solve. First, no compression is applied. In the no compression case, the setup phase computes LU factorizations for all 8000 patches, and the preconditioning apply phase solves the inversion for all 8000 patches using the previously computed LU factors. Second, compression is applied. In this case, the setup phase starts by using Algorithm 3.1 to construct \mathcal{B} with the aforementioned modification. For this problem, \mathcal{B} has exactly 27 entries. After the database is computed, the LU factors are stored in-place instead of strict inverses. The apply phase then applies the 27 stored factorizations against the appropriate choices for the 8000 patches. In each case, we use the LAPACK GETRF and GETRS routines to compute and apply these factorizations, respectively. Table 3 compares timings for the two approaches on a node of the Attaway supercomputer at Sandia.

We observe a slight (9%) speedup in the setup phase of the Compression case because it computes 27 factorizations as opposed to 8000 factorizations, which outweighs the cost of repeatedly computing $\|A_i - B_j\|_{\ell_1}$ for the compression. We suspect that our current implementation of Algorithm 3.1 could be improved for larger database sizes by using a logarithmic search algorithm as discussed earlier. Despite these limitations, there is a significant (23.4%) speedup in the apply phase when compression is utilized even with our simple implementation. We believe this is due to increased data locality by accessing only 27 factorizations of size 216×216 as opposed to accessing 8000 factorizations of size 216×216 . Assuming 8 bytes per value, this corresponds to a difference of storing approximately 9.6MB of dense patch factorizations and 62.5KB of database lookup indices in the compressed case versus 2.8GB of dense patch factorizations in the uncompressed case. To put this in perspective, the cheapest smoother to store explicitly is the Jacobi method, which would require storing 7.9MB of data to

store the diagonal of the 1030301×1030301 matrix for this problem. We also remark that our implementation has plenty of room for performance enhancements, and these numbers should be considered a lower bound for potential benefits. For example, we believe it would be much better to simultaneously solve all patch problems within the same cluster (which we are not currently doing) and the patch matrix could be loaded once in memory and then used for the multiple right hand sides. Additionally, we expect problems with larger patches will be solved with even larger performance gains over approaches with no compression due to the cost scaling of inverting patches. Finally, we note that for linear problem sequences (e.g., within nonlinear solvers or time stepping schemes), setup times can probably be amortized by incorporating some reuse of database assignments from the previous linear setup.

Experiment 4 Nonlinear shock dynamics. We close this section with an example of a nonlinear system with a shock formation. This example utilizes Burgers’ equation

$$\frac{du}{dt} + \nabla \cdot \left(\frac{1}{2} \vec{v} u^2 - \epsilon(\vec{x}) \nabla u \right) = f(\vec{x}).$$

with advection \vec{v} , entropy viscosity strength ϵ . Additional terms for SUPG stabilization are present but not shown. We focus on the case where a shock develops in the primary variable u , using $\vec{v} = [1, 1]^T$. At the final time indicated by the center image of Figure 5, we extract the matrix and analyze the system for compressibility using Algorithm 3.1.

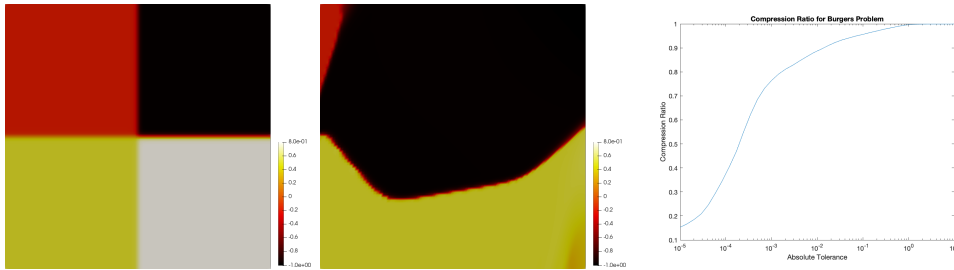


FIG. 5. Burgers’ equation from initial condition $t = 0$ (left) to shock formation at final time $t = 1$ (center) and the associated compressibility curve at final time based on Algorithm 3.1 (right) on a 100×100 mesh with $p = 2$.

In particular, we do not solve the system; however, we use this experiment to demonstrate how patch compressibility behaves for much more complex nonlinear physics. That is, the right image is a plot of $\frac{n_p - \|\mathcal{B}\|}{n_p}$ for a wide range of values of ϵ . It is important to note that compression ratios as high as 90% may be achieved with a tolerance on the order of $\epsilon = 10^{-2}$, meaning this approach is likely applicable to a broad range of problems.

This approach may be extended to Algorithm 3.2 by plotting a clustering quality measure such as cluster variance as a function of number of clusters, which will help identify how amenable a system is to the algorithms in this paper. Additionally not shown, one may plot a histogram of the mapping $\phi()$ to identify the distribution of structure for a given matrix. For example, a histogram for $\phi()$ related to Experiment 2 would show large peaks corresponding to the interior of the constant regions, indicating the problem is largely structured with the exception of interfaces.

5. Conclusion. Two families of algorithms have been presented for detecting and exploiting structure in a linear system for patch preconditioners based on the idea that similar patches can share the same factorization when solving the small patch subproblems. We have illustrated that on some examples, it is possible to maintain similar convergence rates even when the number of stored/factored patches is less than five percent of the number of true patches. This gain makes a more accurate patch-based approach more competitive with inexpensive Jacobi methods, which require very little additional storage (specifically only the matrix diagonal). This is essential in matrix-free applications where often a matrix-free approach is adopted due significant storage concerns. Previously, matrix-free storage advantages are often lost when all patches are stored/factored, as the memory needed to store all patch factorizations is often comparable to the storage needed for the discretization matrix. Now, by only factoring a small subset of the patch matrices, the storage advantages of a matrix-free approach are once again possible. While our focus has been on storage reduction, we have presented some results hinting that it may be possible to reduce run time using a patch compression approach even when a matrix-free approach is not being used. However, additional work is needed to truly demonstrate this. The algorithms presented in this paper are limited in terms of both their implementation and their sophistication. More sophisticated algorithms should be considered to reduce the run time during the setup phase when defining the patch clusters and to reduce the run time in the apply phase when repeatedly solving the same patch matrix system with many different right hand sides. Additionally, more sophisticated clustering algorithms should be considered to improve the quality of the clustering perhaps leveraging ideas that combine clustering algorithms with deep learning algorithms.

The authors would like to thank Nicholas Moore for valuable discussions and feedback. This work was supported by the U.S. Department of Energy, Office of Science, Office of Advanced Scientific Computing Research, Applied Mathematics program and Sandia National Laboratories Laboratory Directed Research & Development Program. Sandia National Laboratories is a multimission laboratory managed and operated by National Technology and Engineering Solutions of Sandia, LLC., a wholly owned subsidiary of Honeywell International, Inc., for the U.S. Department of Energy’s National Nuclear Security Administration under grant DE-NA-0003525. This paper describes objective technical results and analysis. Any subjective views or opinions that might be expressed in the paper do not necessarily represent the views of the U.S. Department of Energy or the United States Government.

REFERENCES

- [1] J. ADLER, T. BENSON, E. CYR, P. FARRELL, S. MACLACHLAN, AND R. TUMINARO, *Monolithic multigrid methods for magnetohydrodynamics*, accepted for publication in SIAM J. on Sci. Comput., (2021). <https://arxiv.org/abs/2006.15700>.
- [2] D. ARNOLD, R. FALK, AND R. WINTHER, *Multigrid in $h(\text{div})$ and $h(\text{curl})$* , Numer. Math., 85 (2000), pp. 197–217.
- [3] A. BARALDI AND P. BLONDA, *A survey of fuzzy clustering algorithms for pattern recognition.*, IEEE Transactions on Systems, Man, and Cybernetics, Part B (Cybernetics), 29 (1999), pp. 778–785.
- [4] P. BASTIAN, M. BLATT, AND R. SCHEICHL, *Algebraic multigrid for discontinuous galerkin discretizations of heterogeneous elliptic problems*, Numerical Linear Algebra with Applications, 19 (2012), pp. 367–388.
- [5] G. BECKER, C. SIEFERT, R. TUMINARO, H. SUN, D. VALIVETI, A. MOHAN, J. YIN, AND H. HUANG, *High resolution viscous fingering simulation in miscible displacement using a p -adaptive discontinuous galerkin method with algebraic multigrid preconditioner*, Jour-

- nal of Computational Physics, 374 (2018), pp. 495–514.
- [6] T. BENSON, J. ADLER, E. CYR, S. MACLACHLAN, AND R. TUMINARO, *Monolithic multigrid methods for two-dimensional resistive magnetohydrodynamics*, SIAM J. Sci. Comput., 38 (2016), pp. B1–B24.
 - [7] M. BENZI, G. GOLUB, AND J. LIESEN, *Numerical solution of saddle point problems*, Acta Numer., 14 (2005), pp. 1–137.
 - [8] P. BRUBECK AND P. FARRELL, *A scalable and robust vertex-star relaxation for high-order fem*, SIAM Journal on Scientific Computing, 44 (2022), pp. A2991–A3017.
 - [9] M. CARON, P. BOJANOWSKI, A. JOULIN, AND M. DOUZE, *Deep clustering for unsupervised learning of visual features*, in Proceedings of the European conference on computer vision (ECCV), 2018, pp. 132–149.
 - [10] P. E. FARRELL, Y. HE, AND S. P. MACLACHLAN, *A local Fourier analysis of additive Vanka relaxation for the Stokes equations*, Numerical Linear Algebra with Applications, 28 (2021), p. e2306.
 - [11] P. E. FARRELL, M. G. KNEPLEY, L. MITCHELL, AND F. WECHSUNG, *Pcpatch: software for the topological construction of multigrid relaxation methods*, arXiv preprint arXiv:1912.08516, (2019).
 - [12] F. FERRACCIOLI AND G. MENARDI, *Modal clustering of matrix-variate data*, Advances in Data Analysis and Classification, (2022), pp. 1–23.
 - [13] A. FRIEZE, R. KANNAN, AND S. VEMPALA, *Fast monte-carlo algorithms for finding low-rank approximations*, Journal of the ACM, 51 (2004), pp. 1025–1041.
 - [14] M. P. GALLAUGHER AND P. D. MCNICHOLAS, *Finite mixtures of skewed matrix variate distributions*, Pattern Recognition, 80 (2018), pp. 83–93.
 - [15] Y. HE AND S. P. MACLACHLAN, *Local fourier analysis for mixed finite-element methods for the stokes equations*, Journal of Computational and Applied Mathematics, 357 (2019), pp. 161–183.
 - [16] J. HEYS, T. MANTEUFFEL, S. F. MCCORMICK, AND L. OLSON, *Algebraic multigrid for higher-order finite elements*, Journal of computational Physics, 204 (2005), pp. 520–532.
 - [17] T. G. KOLDA AND B. W. BADER, *Tensor decompositions and applications*, SIAM review, 51 (2009), pp. 455–500.
 - [18] S. P. MACLACHLAN AND C. W. OOSTERLEE, *Local Fourier analysis for multigrid with overlapping smoothers applied to systems of PDEs*, Numer. Linear Alg. Appl., 18 (2011), pp. 751–774.
 - [19] L. OLSON, *Algebraic multigrid preconditioning of high-order spectral elements for elliptic problems on a simplicial mesh*, SIAM Journal on Scientific Computing, 29 (2007), pp. 2189–2209.
 - [20] Y. QING HUANG, S. SHU, AND X. JUN YU, *Preconditioning higher order finite element systems by algebraic multigrid method of linear elements*, Journal of Computational Mathematics, 24 (2006), pp. 657–664.
 - [21] E. M. RÖNQVIST AND A. T. PATERA, *Spectral element multigrid. i. formulation and numerical results*, Journal of Scientific Computing, 2 (1987), pp. 389–406.
 - [22] C. SIEFERT, R. TUMINARO, A. GERSTENBERGER, G. SCOVAZZI, AND S. COLLIS, *Algebraic multigrid techniques for discontinuous galerkin methods with varying polynomial order*, Computational Geosciences, 18 (2014), pp. p597–612.
 - [23] S. P. VANKA, *Block-implicit multigrid solution of Navier-Stokes equations in primitive variables*, J. Comput. Phys., 65 (1986), pp. 138–158.